In Situ Activation of Nitrogen-Doped Graphene Anchored on Graphite Foam for a High-Capacity Anode

Junyi Ji,[†] Jilei Liu,[‡,∥] Linfei Lai,[‡,∥] Xin Zhao,[§] Yongda Zhen,[‡] Jianyi Lin,[‡] Yanwu Zhu,[⊥] Hengxing Ji,[⊥] Li Li Zhang,[*,‡] and Rodney S. Ruoff[#]

[†]College of Chemical Engineering, Sichuan University, Chengdu, Sichuan 610065, China, [‡]Institute of Chemical and Engineering Sciences, A*STAR, 1 Pesek Road, Jurong Island, 627833 Singapore, [§]College of Material Science & Engineering, State Key Laboratory for Modification of Chemical Fibers and Polymer Materials, Donghua University, Shanghai 201620, China, [∥]Division of Physics and Applied Physics, School of Physical and Mathematical Sciences, Nanyang Technological University, 21 Nanyang link, SPMS-PAP-03-18A, 637371 Singapore, [⊥]Department of Materials Sciences and Engineering, University of Science and Technology of China, Hefei, Anhui 230026, China, and [#]Center for Multidimensional Carbon Materials (CMCM), Institute for Basic Science (IBS) Center at the Ulsan National Institute of Science & Technology (UNIST) Campus, Department of Chemistry and School of Materials Science, UNIST, Ulsan 689-798, Republic of Korea

ABSTRACT We report the fabrication of a three-dimensional free-standing nitrogen-doped porous graphene/graphite foam by *in situ* activation of nitrogen-doped graphene on highly conductive graphite foam (GF). After *in situ* activation, intimate "sheet contact" was observed between the graphene sheets and the GF. The sheet contact produced by *in situ* activation is found to be superior to the "point contact" obtained by the traditional drop-casting method and facilitates electron transfer. Due to the intimate contact as well as the use of an ultralight GF current collector, the composite electrode delivers a gravimetric capacity of 642 mAh g^{-1} and a volumetric capacity of 602 mAh cm^{-3} with respect to the whole electrode mass and volume (including the active materials and the GF current collector). When normalized based on the mass of the active material, the composite electrode delivers a high specific capacity of up to 1687 mAh g^{-1}, which is superior to that of most graphene-based electrodes. Also, after ~90 s charging, the anode delivers a capacity of about 100 mAh g^{-1} (with respect to the total mass of the electrode), indicating its potential use in high-rate lithium-ion batteries.

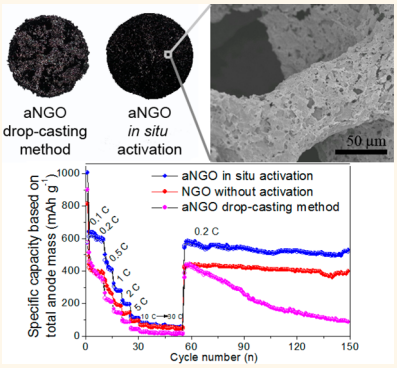

KEYWORDS: *in situ* activation · sheet contact · lithium-ion battery · nitrogen-doped graphene · graphite foam

Lithium-ion batteries (LIBs) with large energy density, high power density, and long lifespan are necessary in many applications, such as consumer electronics and electric vehicles.[1] A classical graphite anode has a limited theoretical capacity of 372 mAh g^{-1}. Thus, tremendous effort has been devoted to the preparation of advanced anode materials with improved energy and power densities to meet the ever-increasing high-energy needs of technological applications.[2] Graphene-based anodes have attracted a great deal of attention owing to their high intrinsic surface area, high electrical conductivity, and ability to reversibly store lithium, not only on both sides of the graphene but also on its edges and defect sites.[3−6] In addition, chemical dopants/functional groups have been proven both experimentally and theoretically to significantly increase the reversible lithium storage.[7−13] First-principles studies have predicted that the reversible capacity of a pyridinic structure can reach 1262 mAh g^{-1}.[10] Another theoretical prediction based on reversible electrochemical lithium addition to C_6 aromatic rings with a Li_6C_6 model gives discharge capacities of up to 2000 mAh g^{-1}.[11]

Though many research groups have reported graphene-based anodes with a high specific capacity,[7,8,14−19] the values are usually based on only the mass of the active materials, and the loading of the active materials is generally small (<0.5 mg cm^{-2}). However, when the total electrode mass, including the current collector, is taken into consideration (for a commercial Cu current collector, this is about 16 mg cm^{-2}), the specific capacity based on the whole electrode mass is limited. Thus, to improve the true performance of an anode on a total electrode basis (both mass and volume), increasing the loading of

* Address correspondence to zhang_lili@ices.a-star.edu.sg.

Received for review June 25, 2015 and accepted August 10, 2015.

Published online August 10, 2015
10.1021/acsnano.5b03888

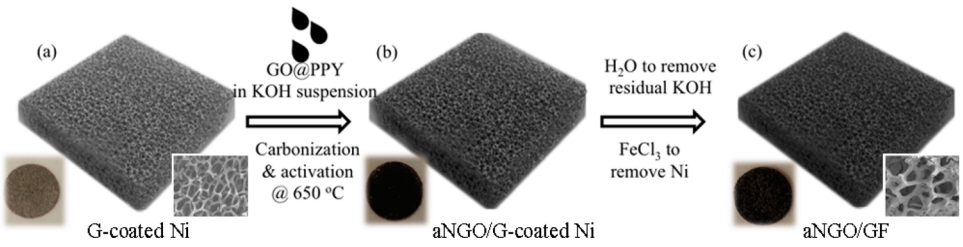

Figure 1. Illustration of the fabrication of the aNGO/GF electrode: (a) G-coated Ni substrate, (b) infiltration of the G-coated Ni substrate with a GO@PPY in KOH suspension and carbonization and activation at 650 °C to obtain aNGO/G-coated Ni, and (c) final aNGO/GF obtained after residual KOH and Ni removal by DI water and 0.5 M $FeCl_3$, respectively.

active materials and/or decreasing the weight of the current collector are efficient methods.[2,20−24]

Here, by *in situ* fabrication, we present a three-dimensional (3D) free-standing nitrogen-doped porous graphene/graphite foam anode, which achieves large gravimetric and volumetric capacities of 642 mAh g^{-1} and 602 mAh cm^{-3}, respectively, on a whole electrode basis, with good rate capability and cycling stability. The values are obtained with an anode having a large active mass loading (the active material is 65 wt %). With ∼90 s charging time, the anode can deliver a significant capacity of 102 mAh g^{-1}, indicating its promising use as a high-rate LIB anode. The high specific capacity and good rate capability based on the whole electrode mass are attributed to the intimate "sheet contact" between the active material and the graphite foam current collector that facilitates the charge transfer rate.

RESULTS AND DISCUSSION

Figure 1 illustrates the *in situ* fabrication process of the 3D free-standing nitrogen-doped porous graphene/graphite foam electrode. A thin graphitic layer of carbon coating the Ni foam (G-coated Ni) was prepared by our previously reported method.[25] Graphene oxide encapsulated in polypyrrole (GO@PPY) was synthesized by an oxidative template route.[26] A mixture of KOH in ethanol was then added dropwise to a suspension of GO@PPY in ethanol. The G-coated Ni was then infiltrated with the suspension (GO@PPY and KOH in ethanol) and dried. *In situ* carbonization and activation were then carried out by placing the material in a horizontal quartz tube furnace under an argon flow at 650 °C and a pressure of 1 atm for 30 min. The product from this step is a composite of activated GO@PPY in G-coated Ni (which we refer to as aNGO/G-coated Ni; the GO@PPY is fully converted to N-doped carbon after the activation process). The final free-standing material, denoted as aNGO/GF, where GF now refers to the graphite or multilayer graphene foam, was obtained after washing with deionized (DI) water to remove the residual KOH and 0.5 M $FeCl_3$ to remove the Ni, followed by drying in a vacuum at 80 °C for 12 h. The amount of active material, which is the aNGO in the aNGO/GF, can be controlled during the infiltration step. Various mass loadings ranging from ∼20 to 75 wt % were prepared. Photographs of the G-coated Ni, aNGO/G-coated Ni, and aNGO/GF are shown in Figure S1. The final product aNGO/GF preserves the shape and size of the original G-coated Ni. Compared to other activated carbon products, the aNGO/GF with an inactive yet lightweight GF support can provide a free-standing 3D interconnected structure, and the relatively high mechanical strength of GF makes it suitable to act as the electrode without additional support.

The X-ray diffraction (XRD) pattern of the pure GF shows well-resolved diffraction peaks that are in good agreement with the standard pattern of graphite (Figure 2a).[25] The (002) peak of aNGO powder (activated without the G-coated Ni substrate) is significantly reduced and broadened, indicating the presence of predominately single- or few-layer "graphene" sheets.[27] The XRD pattern of the aNGO/GF consists of both the diffraction peaks of the GF and the aNGO, indicating the presence of both components and that their crystalline structure is not affected in the composite material. In addition, no diffraction peaks associated with Ni are seen for aNGO/GF, implying the complete or almost complete removal of Ni. XPS survey scan spectra (Figure 2b) show the presence of C, O, and N in both aNGO and aNGO/GF, and the inset shows the C 1s spectra of the two samples. The position of the main C 1s peak at 284.6 eV confirms that sp^2 C−C bonding is present in the aNGO/GF. The tail between 286.0 and 290.0 eV in both samples is due to the oxygen- and nitrogen-containing functional groups. The nitrogen content in the aNGO/GF is around 2−3 atom %. Deconvolution of the N 1s peaks (Figure 2c) indicates three types of N, pyrrolic N (N5), pyridinic N (N6), and graphitic N (NQ).[28] Pyrrolic N is the main N-containing functional group since the nitrogen came from polypyrrole, and the carbonization was carried out at a relatively low temperature (650 °C). Nitrogen adsorption/desorption analysis (Figure 2d) indicates a specific surface area (SSA) of about 2123 m^2 g^{-1} for the aNGO powder. The SSA of the aNGO/GF increases with an increasing percentage of the active material (Figure S2), and a measured SSA for the aNGO/GF of 943 m^2 g^{-1} with a mass loading of 70 wt % aNGO was obtained. Moreover, the blue shift of the G band and significant D band in the Raman spectra confirms the conversion of the polypyrrole to a N-doped carbon

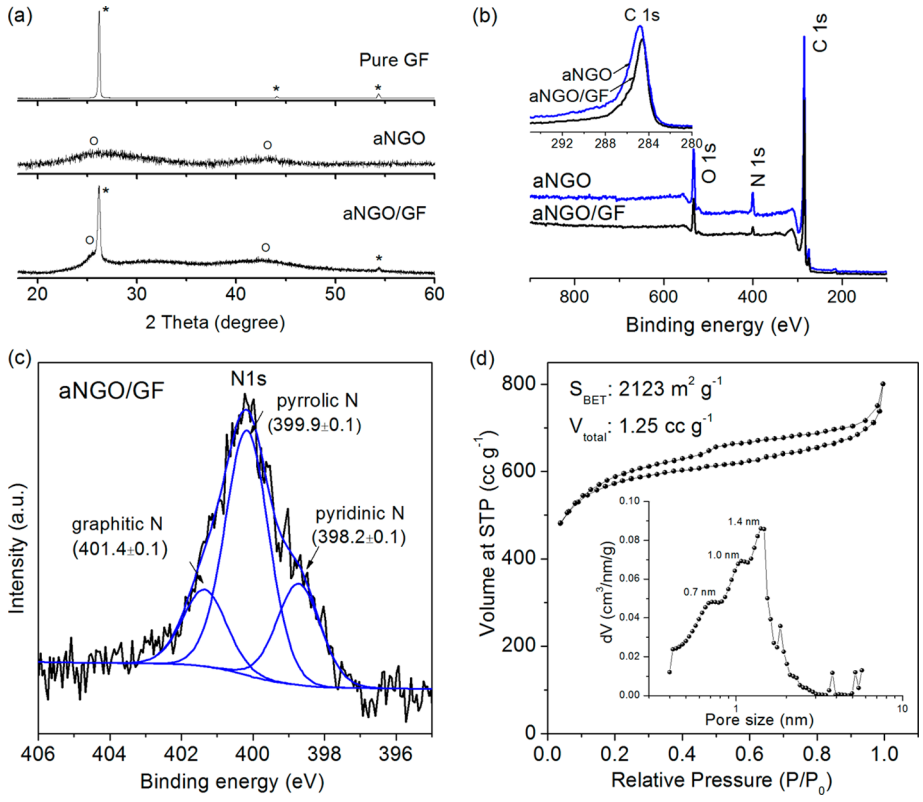

Figure 2. (a) XRD patterns of GF, aNGO, and aNGO/GF; (b) XPS spectra of aNGO and aNGO/GF; (c) XPS N 1s spectrum of aNGO/GF; and (d) nitrogen sorption of aNGO.

and thus the nitrogen doping of the graphene sheets after activation (Figure S3).[29,30]

Scanning electron microscopy (SEM) images show that the aNGO/GF has preserved the 3D interconnected network structure of the pure GF (Figure 3a,b) and for the aNGO shows a continuous and uniform distribution on the GF struts. During activation, the molten KOH reacts with the carbon to generate nanoholes and rearranges the carbon. The resulting restructuring yields a distribution of meso- and micropore channels and increases the specific surface area.[27] Moreover, the continuous distribution of the aNGO is strongly influenced by the structure of the GO@PPY/KOH precursor film as well as the relatively uniform distribution of KOH nanoparticles between the GO@PPY layers that was introduced prior to activation.[31] The open structure seen in Figure 3c shows that the outer surface of the GF struts was covered by the activated graphene (aNGO). A high-magnification SEM image (inset of Figure 3c) and a TEM image (Figure 3d) reveal curled and overlapping activated graphene sheets uniformly covering the GF struts. Furthermore, intimate contact between the aNGO sheets and the GF can be seen in Figure 3g. A thin layer of aNGO covered the GF surface and remained as a "sheet contact" with the GF. For comparison, we prepared another two electrodes. One was obtained by drop-casting the aNGO powder onto the GF with a binder (aNGO-on-GF), and the other was obtained without KOH activation during carbonization (NGO-GF). Both the aNGO-on-GF and NGO-GF show a highly crumpled and discontinuous distribution of active materials (Figures 3f and S4d−i). In addition, contact between the crumpled active material and GF for aNGO-on-GF and NGO-GF is more "point contact", while that of the aNGO/GF is "sheet contact" (Figure 3g−i). The contact between the active material and the current collector plays a very important role in the electrochemical performance. Good contact and continuous distribution results in efficient charge transfer between the current collector and the active material. These results imply the following roles of KOH: (1) it acts as an activating agent to generate small pores in the activated graphene sheets, and (2) the *in situ* KOH activation ensures continuous distribution of the active material and intimate contact between the activated graphene sheets and the GF surface through the chemical activation process. When the mass loading of aNGO is increased, the activated graphene sheets tend to partially fill the pores of the GF (Figure S4b). This partial filling not only increases the density of the aNGO/GF, it also increases the active fraction of the electrode, resulting in better gravimetric and volumetric capacities on a total electrode basis. The density of the aNGO/GF anode tested after compression was up to 1 g cm^{-3} with an areal density of up to 4 mg cm^{-2}. The direct activation and carbonization of the aNGO on GF produces intimate contact and strong binding between the active material (aNGO) and the

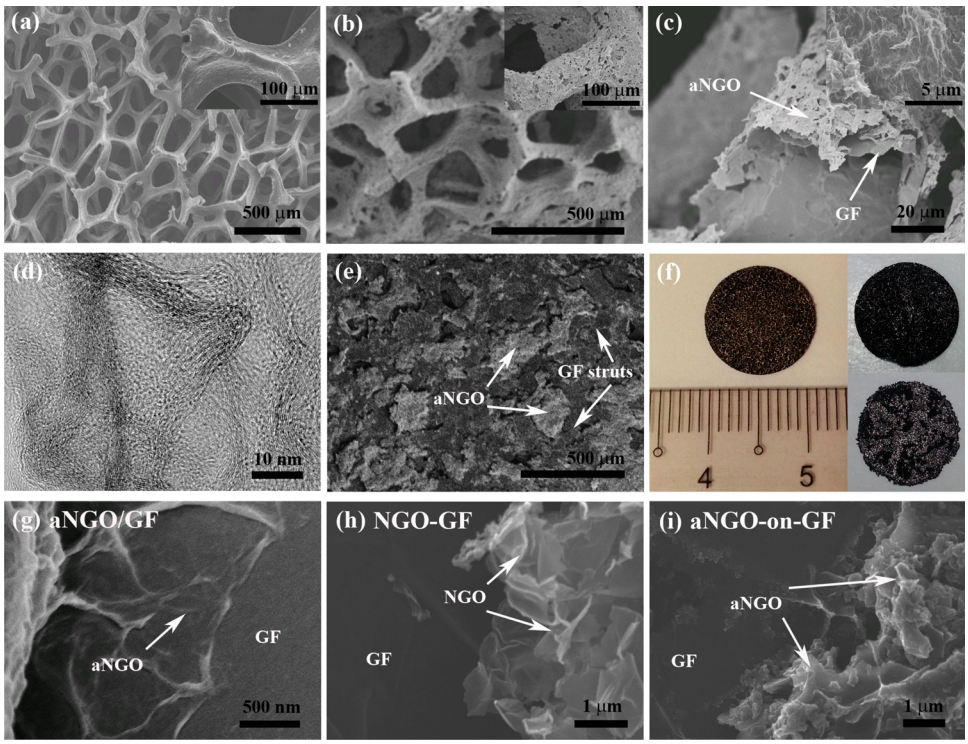

Figure 3. SEM images of (a) pure GF, (b,c) aNGO/GF at different magnifications, (d) TEM image of aNGO/GF, (e) SEM images of aNGO/GF after compression under 30 kN, and (f) photographs of aNGO/GF (left and right top) and aNGO-on-GF (right bottom) after compression. Active mass loadings are 1 and 0.9 mg cm^{-2}, respectively. SEM images of (g) aNGO/GF, (h) NGO-GF, and (i) aNGO-on-GF.

current collector (GF). When compressed at 30 kN, the GF struts remained continuous and were fully covered by the aNGO. No aNGO peels off the GF (Figure 3e and Figure S4c).

The performance of aNGO/GF as an anode for LIBs is shown in Figure 4. It should be noted that this is based on the total mass of the anode (including the mass of activated graphene and GF), not the mass of active material only. Furthermore, the aNGO/GF was used directly as the anode, without the use of a metal current collector, binder, and carbon black. Cyclic voltammograms (CV) for the first three cycles obtained at a scan rate of 0.1 mV s^{-1} in the potential range of 0.01−3.0 V are shown in Figure 4a. The first cathodic scan shows an obvious peak in the potential range of 0.4−0.8 V that disappeared in subsequent cycles. The peak is attributed to the formation of solid electrolyte interphase (SEI) films.[32−35] Disappearance of this peak in the subsequent scans suggests the existence of a stable SEI film that prevents further contact between the electrolyte and the anode. The peaks in the second and third cycles are, respectively, centered at about 0.01 and 0.15 V in the cathodic scan and 0.24 and 0.29 V in the anodic scan and are due to the intercalation of lithium ions in the graphite foam.[33−36] A capacitive region is observed from 1.5 to 3.0 V.[33] In both CV and charge/discharge curves (Figure 4a,b), the capacity below 0.5 V is due to the reversible lithium intercalation in the thin graphene layers,[36−38] while the capacity between 0.5 and 1.5 V is related to the reversible lithium insertion/extraction from the residual functional groups, pores, and edges of the graphene layers.[4−6,17,39,40]

The aNGO/GF anodes with different active mass loadings were tested to investigate their charge/discharge rate capability and stability (Figure 4c−e). When the total mass of the anode is considered in evaluating the true performance of a half cell, the percentage of active material plays an important role; here, this means that in a certain percentage range, the more active the material, the higher the specific capacity. Figure 4c shows that when the loading of aNGO increased from about 50 to 70 wt %, both the gravimetric and volumetric capacities based on the total anode mass and volume increased at all scan rates. However, there might be a trade-off in terms of the specific capacity and rate capability/stability. When the mass loading of the active material approaches and exceeds about 70 wt %, the specific capacity at C rates above 10 C decreases. In addition, the stability at 0.2 C was also found to decrease when the active mass loading is too high, and here, this was found to be about 70 wt % of the active materials.

Based on the above discussion, an active loading of no more than 70 wt % should have a good balanced performance between specific capacity, rate capability, and stability. At 0.1 C, the specific capacity of the aNGO/GF anode based on the total mass of the electrode is about 642 mAh g^{-1} (volumetric capacity is

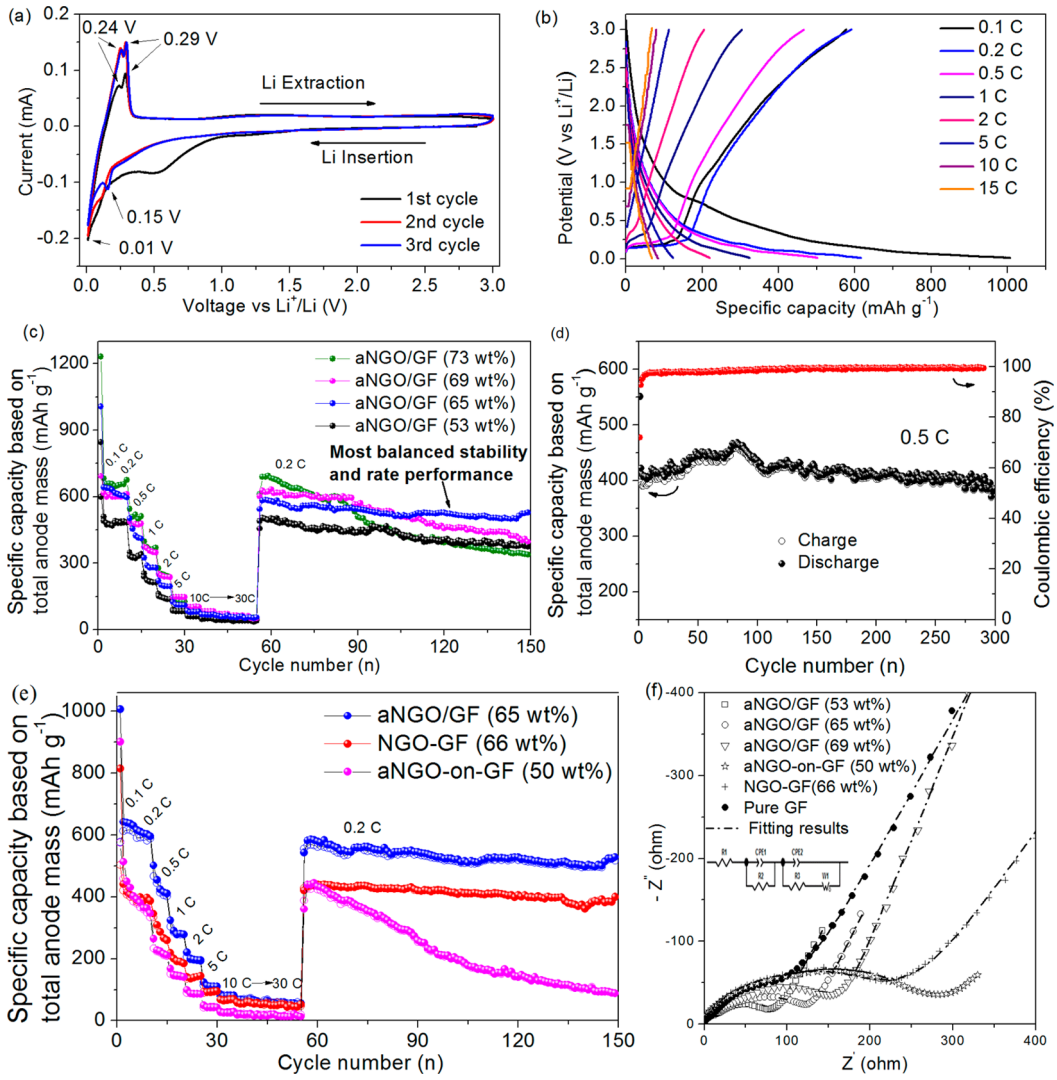

Figure 4. Electrochemical performance of various anodes based on the total electrode mass. (a) CV at a scan rate of 0.1 mV s^{-1}, (b) charge/discharge curves of aNGO/GF (65 wt %) anode at different current densities, (c) specific capacity of various aNGO/GF anodes during cycling at different current densities, (d) cycling and Coulombic efficiency aNGO/GF (65 wt %) at a current density of 0.5 C, (e) comparison of anodes prepared with different methods during cycling at different current densities, and (f) Nyquist plots of various anodes with the fitting results.

~602 mAh cm^{-3}, 65 wt %). When the current rate was increased to as high as 10 C (corresponding to a charge time of ~90 s), a specific capacity of about 102 mAh g^{-1} and a volumetric capacity of about 96 mAh cm^{-3} were obtained on a total electrode basis (69 wt % of aNGO load mass ratio). Furthermore, the specific capacity was recovered once the current density was restored to 0.2 C, implying good reversibility of the anode. These results are, to the best of our knowledge, better than most of those for carbon, graphene, silicon, and metal-oxide-based anodes reported in the literature when the mass of the whole electrode is considered.[6−9,13,14,17,41−45] This is due to the extremely low density of the current collector (GF), which also contributes to the total capacity through lithiation/delithiation within a thin layer of graphite. In addition, the aNGO/GF anode shows good cycling stability (Figure 4d). At a current rate of 0.5 C, the anode maintains a high capacity of 397 mAh g^{-1} after 300 cycles with a Coulombic efficiency of almost 100%. Although the specific capacity of the aNGO/GF anode is smaller than that of Si-based anodes at a low current rate,[45] the rate capability and the cycling stability of the aNGO/GF anode significantly outperform Si-based anodes, making, in our opinion, aNGO/GF a promising anode for high-performance LIBs.

The performance of the aNGO-on-GF and the NGO-GF anodes was also investigated and compared with that of the aNGO/GF anode (Figure 4e). With a similar loading of active material, aNGO-on-GF shows poor stability. On the other hand, the NGO-GF anode exhibits a specific capacity smaller than that of the aNGO/GF. This can be attributed to the poor contact between the active material and the current collector, as shown by the SEM images (Figures 3g−i and S4c−i) and the impedance analysis (Figure 4f). Electrochemical impedance spectroscopy (EIS) was used to provide

TABLE 1. Fitting Results of Various Anodes Based on the Equivalent Electric Circuit (in Figure 4f)

samples	R_{SEI} (ohm)	CPE-P (SEI)	R_{CT} (ohm)	CPE-P (CT)
aNGO/GF (53 wt %)	21.3	0.75	46.2	0.86
aNGO/GF (65 wt %)	48.4	0.75	60.7	0.84
aNGO/GF (69 wt %)	53.7	0.68	82.4	0.86
aNGO-on-GF (50 wt %)	55.6	0.75	194	0.64
NGO-GF (66 wt %)	42.5	0.85	124	0.71
pure GF	24.2	0.67	26.1	1

information on the resistance of different anodes. Nyquist plots and their respective fittings with an appropriate electric equivalent circuit are shown in Figure 4f and Table 1. For the aNGO/GF anodes, the total resistance increases with the increase of active mass, mainly due to the increase of charge transfer resistance (R_{CT}). With a similar active mass loading, the charge transfer resistances of the aNGO-on-GF (194 ohm) and the NGO-GF (124 ohm) are much larger than that of the aNGO/GF (46 ohm), indicating a much slower charge transfer rate for the aNGO-on-GF and NGO-GF anodes. The different contact modes ("point contact" for the NGO-GF and aNGO-on-GF anodes and "sheet contact" for the aNGO/GF anode) between the active material and the current collector, as well as the difference in porosity and defect density of the active material, could account for the different capacitive performances of the anodes. SEM images of the aNGO/GF and NGO-GF anodes after long-time cycling are shown in Figure S5. Both show intimate contact after cycling. No peeling off or disassembly of the active materials is observed. The sheet contact between aNGO and GF and the point contact between NGO and GF remain after the cycling tests. This further confirms the highly stable performance of the anodes to cycling.

For the sake of comparison with other studies, the performance of the anodes based on the mass of active material (*i.e.*, the mass of aNGO) was also measured. With an areal loading of 1.5 mg cm^{-2} (~24 wt %), the specific capacity of aNGO/GF anode is 2321 mAh g^{-1} at a current rate of 0.1 C (Figure S6a). This greater than theoretical value is due to the capacity contribution from the GF, whose mass is not included in the capacity calculation. A rough estimate of the contribution from the GF, based on the reversible specific capacity of pure GF (Figure S6b), is about 27%, and thus the calculated specific capacity from the active material is about 1687 mAh g^{-1} (at 0.1 C). This capacity value is still higher than that for the other carbon/graphene-based anodes and approaches the predicted theoretical value based on a Li_6/C_6 model.[11] The improved electrochemical performance of the aNGO/GF anode compared with that of other graphene-based anodes is attributed to its well-designed structure: (1) the intimate and continuous contact between the active material and the current collector ensures efficient electron transfer; (2) an open three-dimensional structure with thin graphitic layers facilitates ion transport within the electrode with small diffusion resistance; (3) the uniform coverage of the GF by thin and porous graphitic layers (aNGO) forms a rigid framework, which is structurally stable during repeated lithiation/delithiation even at high rates; (4) nitrogen-containing functional groups increase the specific capacity; (5) the direct activation of the active material on an ultralight GF current collector improves the rate performance of the anode but also reduces the inert mass in the anode, thus resulting in a high specific capacity of the whole anode; (6) the ability to accommodate up to 70 wt % of the active material in the anode (without the use of binder and conducting carbon additives) without significant deterioration of the overall performance is very favorable in terms of both gravimetric and volumetric capacities on a total electrode basis.

SUMMARY

We have developed a novel *in situ* activation method to fabricate 3D free-standing nitrogen-doped porous graphene/graphite foam anodes. The KOH *in situ* activation not only generates small pores in graphene sheets but also ensures intimate "sheet contact" between the activated graphene sheets and the GF surface. The aNGO/GF anode delivered a gravimetric capacity of 642 mAh g^{-1} and a volumetric capacity of 602 mAh cm^{-3} on a total electrode basis with good rate capability and stability. With 90 s of charging, the aNGO/GF anode is able to deliver a capacity of about 100 mAh g^{-1} (with respect to the total mass of the electrode), indicating its promising use as a high-rate LIB anode.

EXPERIMENTAL SECTION

Preparation of the GO@PPY in KOH Suspension. Graphene oxide encapsulated in polypyrrole (denoted GO@PPY) was first synthesized by an "oxidative template" route. Pyrrole was distilled twice prior to use. The colloidal dispersion of graphene oxide (GO) flakes was prepared by the sonication of graphite oxide (G-O), which was obtained from natural graphite (Bay Carbon, Inc., SP-1) using a modified Hummers method. Cetrimonium bromide (0.5 g) was dissolved in HCl (1 M, 10 mL) and was added to a GO (1.3 mg mL^{-1}, 20 mL) dispersion under constant stirring in an ice bath. Then ammonium persulfate (0.9 g) was added. After 30 min, pyrrole monomer (0.5 g) was added to the above solution. The reaction was carried out at 0−5 °C for 24 h while it was shielded from light. A black precipitate (GO@PPY) was formed and removed by filtering using a polycarbonate membrane (Whatman, 0.2 μm). The filtrate was thoroughly washed with ethanol followed by DI water. It was then dried at 80 °C for 24 h in an oven. The dried GO@PPY (100 mg) was then added to ethanol (50 mL) under sonication for 30 min to produce a

TABLE 2. Mass of the G-Coated Ni before and after KOH Activation

sample	empty GF/Ni	after activation and washing
G-coated Ni-1	27.7	27.7
G-coated Ni-2	28.4	28.4
G-coated Ni-3	42.4	42.4

suspension. At the same time, a solution of KOH in ethanol was prepared, which was then added dropwise to the GO@PPY suspension until the weight ratio of GO@PPY to KOH was 1:3. The resulting GO@PPY in KOH suspension was used to infiltrate the G-coated Ni foam.

Synthesis of the aNGO/GF Composite. A thin graphite coating on Ni foam (G-coated Ni) was prepared as previously reported.[25] The GO@PPY in KOH suspension was drop-cast onto the G-coated Ni substrate on a hot plate heated to 90 °C. After the solvent had evaporated, another drop was added. This process was repeated several times until the desired GO@PPY loading was obtained. The hybrid was then placed in a quartz tube furnace under a flow of argon at 650 °C for 30 min at a pressure of 1 atm. The sample was then cooled to room temperature and washed with DI water to remove the residual KOH and 0.5 M $FeCl_3$ to remove the Ni. The final product was dried in a vacuum oven at 80 °C for 12 h and is denoted as aNGO/GF. The mass loading of the aNGO in the aNGO/GF composite was controlled during the infiltration step. For comparison, the GF was infiltrated with the same amount of KOH and annealed under the same conditions. No weight change was observed after washing away the KOH, indicating that the GF was not affected (or affected only slightly) by the activation step. Furthermore, a control experiment showed that the weight of the GF was not changed after the KOH activation process (Table 2).

Synthesis of Pure aNGO Powder. Pure aNGO powder was obtained under the same experimental conditions as used for aNGO/GF, except that no G-coated Ni was used.

Synthesis of the NGO-GF Hybrid. NGO-GF was obtained under the same experimental conditions as used for aNGO/GF, except that no KOH was used.

Preparation of the aNGO-on-GF Hybrid. aNGO powder was mixed with poly(vinyl difluoride) in 1-methyl-2-pyrrolidone with a weight ratio of 80:20 to form a homogeneous slurry under magnetic stirring for 12 h and was then drop-cast onto the graphite foam.

General Characterization. The morphology and microstructure of the samples were analyzed by SEM (JEOL JSM-6700F) and TEM (Tecnai, F20, 200 kV). XPS was performed on a VG ESCALAB 250 spectrometer (Thermo Electron, U.K.) using an Al Kα X-ray source (1486 eV). XRD was done with a Bruker D8 Advance instrument using Cu Kα radiation (λ = 0.154 nm). Brunauer–Emmett–Teller (BET) specific surface areas were obtained by measuring nitrogen adsorption with a Nova Quantachrome (Autosorb-6) at 77.4 K. Raman spectra (Renishaw) were obtained with an excitation laser wavelength of 532 nm.

Electrochemical Characterization. The electrode was assembled in an argon-filled glovebox using a coin-type cell (CR2032) with pure lithium foil (99.9%, Aldrich) as the counter electrode, a polypropylene membrane (Celgard 2400) as the separator, and 1 M $LiPF_6$ in ethylene carbonate and dimethyl carbonate (1:1 by volume, Novolyte) as the electrolyte. All the electrodes were dried at 110 °C under vacuum and then compressed under 30 kN before assembly. The densities of the anode with active material loading of 65 wt % were 0.06 and 0.94 g cm^{-3} before and after the compression, respectively. Note that the goal of the compression with 30 kN is to obtain a dense aNGO/GF anode by reducing the void space but not to adversely affect the structure of the active material. The as-prepared aNGO/GF composite has a large empty space because the GF has a large pore size of several hundred micrometers (the nickel foam is reported to have 42 mg cm^{-2} foam density, 450 μm average pores size, 110 ppi porosity). The electrode is, of course, compressed during the assembly of the coin cell, and the 30 kN compression is smaller than the compression applied during cell assembly. Nitrogen adsorption on the same sample (~40 wt %) before and after 30 kN compression was done to obtain the BET specific surface area and the total pore volume. The BET specific surface areas before and after pressing were about 516 and 477 $m^2 g^{-1}$, respectively. The total pore volumes before and after pressing were about 2.2 and 1.3 mL g^{-1}, respectively. The large reduction in the pore volume is due to the reduction of the empty space of the foam structure upon compression. The BET specific surface area is slightly changed following compression (~7.5% lower). However, compression did not significantly affect the microstructure.

CV data were measured between 0.01 and 3 V at a scan rate of 0.1 mV s^{-1} with a Solartron electrochemical workstation. Galvanostatic charge/discharge cycles were obtained on a Land instrument (CT2001A) in the voltage window between 0.01 and 3 V at room temperature. EIS was carried out by applying a perturbation voltage of 10 mV in the frequency range of 1000 kHz to 10 mHz at open-circuit potential using a Solartron electrochemical impedance analyzer. The current densities used were based on the total mass of the anode, and here, 1 C corresponds to 372 mA g^{-1}.

Conflict of Interest: The authors declare no competing financial interest.

Supporting Information Available: The Supporting Information is available free of charge on the ACS Publications website at DOI: 10.1021/acsnano.5b03888.

Additional characterization data of optical images, SEM images, nitrogen sorption isotherms, Raman spectra, and electrochemical test (PDF)

Acknowledgment. We appreciate the financial support from the Agency for Science, Technology and Research (A*STAR) of Singapore, and the National Natural Science Foundation of China (21490582).

REFERENCES AND NOTES

1. Choi, N. S.; Chen, Z.; Freunberger, S. A.; Ji, X.; Sun, Y. K.; Amine, K.; Yushin, G.; Nazar, L. F.; Cho, J.; Bruce, P. G. Challenges Facing Lithium Batteries and Electrical Double-Layer Capacitors. *Angew. Chem., Int. Ed.* **2012**, *51*, 9994–10024.
2. Zhou, G.; Li, F.; Cheng, H.-M. Progress in Flexible Lithium Batteries and Future Prospects. *Energy Environ. Sci.* **2014**, *7*, 1307–1338.
3. Han, S.; Wu, D.; Li, S.; Zhang, F.; Feng, X. Graphene: A Two-Dimensional Platform for Lithium Storage. *Small* **2013**, *9*, 1173–1187.
4. Wang, C.; Li, D.; Too, C. O.; Wallace, G. G. Electrochemical Properties of Graphene Paper Electrodes Used in Lithium Batteries. *Chem. Mater.* **2009**, *21*, 2604–2606.
5. Pan, D.; Wang, S.; Zhao, B.; Wu, M.; Zhang, H.; Wang, Y.; Jiao, Z. Li Storage Properties of Disordered Graphene Nanosheets. *Chem. Mater.* **2009**, *21*, 3136–3142.
6. Yoo, E.; Kim, J.; Hosono, E.; Zhou, H.-s.; Kudo, T.; Honma, I. Large Reversible Li Storage of Graphene Nanosheet Families for Use in Rechargeable Lithium Ion Batteries. *Nano Lett.* **2008**, *8*, 2277–2282.
7. Wang, H.; Zhang, C.; Liu, Z.; Wang, L.; Han, P.; Xu, H.; Zhang, K.; Dong, S.; Yao, J.; Cui, G. Nitrogen-Doped Graphene Nanosheets with Excellent Lithium Storage Properties. *J. Mater. Chem.* **2011**, *21*, 5430–5434.
8. Wu, Z.-S.; Ren, W.; Xu, L.; Li, F.; Cheng, H.-M. Doped Graphene Sheets As Anode Materials with Superhigh Rate and Large Capacity for Lithium Ion Batteries. *ACS Nano* **2011**, *5*, 5463–5471.
9. Qie, L.; Chen, W. M.; Wang, Z. H.; Shao, Q. G.; Li, X.; Yuan, L. X.; Hu, X. L.; Zhang, W. X.; Huang, Y. H. Nitrogen-Doped Porous Carbon Nanofiber Webs As Anodes for Lithium Ion Batteries with a Superhigh Capacity and Rate Capability. *Adv. Mater.* **2012**, *24*, 2047–2050.
10. Ma, C.; Shao, X.; Cao, D. Nitrogen-Doped Graphene Nanosheets As Anode Materials for Lithium Ion Batteries: A First-Principles Study. *J. Mater. Chem.* **2012**, *22*, 8911–8915.

11. Han, X.; Qing, G.; Sun, J.; Sun, T. How Many Lithium Ions Can Be Inserted onto Fused C6 Aromatic Ring Systems? *Angew. Chem., Int. Ed.* **2012**, *51*, 5147–5141.
12. Wu, D.; Li, Y.; Zhou, Z. First-Principles Studies on Doped Graphene As Anode Materials in Lithium-Ion Batteries. *Theor. Chem. Acc.* **2011**, *130*, 209–213.
13. Shin, W. H.; Jeong, H. M.; Kim, B. G.; Kang, J. K.; Choi, J. W. Nitrogen-Doped Multiwall Carbon Nanotubes for Lithium Storage with Extremely High Capacity. *Nano Lett.* **2012**, *12*, 2283–2288.
14. Reddy, A. L. M.; Srivastava, A.; Gowda, S. R.; Gullapalli, H.; Dubey, M.; Ajayan, P. M. Synthesis of Nitrogen-Doped Graphene Films for Lithium Battery Application. *ACS Nano* **2010**, *4*, 6337–6342.
15. Li, N.; Chen, Z.; Ren, W.; Li, F.; Cheng, H.-M. Flexible Graphene-Based Lithium Ion Batteries with Ultrafast Charge and Discharge Rates. *Proc. Natl. Acad. Sci. U. S. A.* **2012**, *109*, 17360–17365.
16. Li, X.; Geng, D.; Zhang, Y.; Meng, X.; Li, R.; Sun, X. Superior Cycle Stability of Nitrogen-Doped Graphene Nanosheets As Anodes for Lithium Ion Batteries. *Electrochem. Commun.* **2011**, *13*, 822–825.
17. Wang, Z.-L.; Xu, D.; Wang, H.-G.; Wu, Z.; Zhang, X.-B. *In Situ* Fabrication of Porous Graphene Electrodes for High-Performance Energy Storage. *ACS Nano* **2013**, *7*, 2422–2430.
18. Lian, P.; Zhu, X.; Liang, S.; Li, Z.; Yang, W.; Wang, H. Large Reversible Capacity of High Quality Graphene Sheets As an Anode Material for Lithium-Ion Batteries. *Electrochim. Acta* **2010**, *55*, 3909–3914.
19. Wang, G.; Shen, X.; Yao, J.; Park, J. Graphene Nanosheets for Enhanced Lithium Storage in Lithium Ion Batteries. *Carbon* **2009**, *47*, 2049–2053.
20. Stoller, M. D.; Ruoff, R. S. Best Practice Methods for Determining an Electrode Material's Performance for Ultracapacitors. *Energy Environ. Sci.* **2010**, *3*, 1294–1301.
21. Gogotsi, Y.; Simon, P. True Performance Metrics in Electrochemical Energy Storage. *Science* **2011**, *334*, 917–918.
22. De Volder, M. F.; Tawfick, S. H.; Baughman, R. H.; Hart, A. J. Carbon Nanotubes: Present and Future Commercial Applications. *Science* **2013**, *339*, 535–539.
23. Gwon, H.; Hong, J.; Kim, H.; Seo, D.-H.; Jeon, S.; Kang, K. Recent Progress on Flexible Lithium Rechargeable Batteries. *Energy Environ. Sci.* **2014**, *7*, 538–551.
24. Dong, Y.; Liu, S.; Wang, Z.; Liu, Y.; Zhao, Z.; Qiu, J. Compressible Graphene Aerogel Supported CoO Nanostructures As Binder-Free Electrode for High-Performance Lithium-Ion Batteries. *RSC Adv.* **2015**, *5*, 8929–8932.
25. Ji, H.; Zhang, L.; Pettes, M. T.; Li, H.; Chen, S.; Shi, L.; Piner, R.; Ruoff, R. S. Ultrathin Graphite Foam: A Three-Dimensional Conductive Network for Battery Electrodes. *Nano Lett.* **2012**, *12*, 2446–2451.
26. Zhang, L. L.; Zhao, S.; Tian, X. N.; Zhao, X. S. Layered Graphene Oxide Nanostructures with Sandwiched Conducting Polymers As Supercapacitor Electrodes. *Langmuir* **2010**, *26*, 17624–17628.
27. Zhu, Y.; Murali, S.; Stoller, M. D.; Ganesh, K. J.; Cai, W.; Ferreira, P. J.; Pirkle, A.; Wallace, R. M.; Cychosz, K. A.; Thommes, M.; Su, D.; Stach, E. A.; Ruoff, R. S. Carbon-Based Supercapacitors Produced by Activation of Graphene. *Science* **2011**, *332*, 1537–1541.
28. Pels, J.; Kapteijn, F.; Moulijn, J.; Zhu, Q.; Thomas, K. Evolution of Nitrogen Functionalities in Carbonaceous Materials During Pyrolysis. *Carbon* **1995**, *33*, 1641–1653.
29. Ferrari, A. C.; Basko, D. M. Raman Spectroscopy As a Versatile Tool for Studying the Properties of Graphene. *Nat. Nanotechnol.* **2013**, *8*, 235–246.
30. Hu, H.; Zhao, Z.; Wan, W.; Gogotsi, Y.; Qiu, J. Polymer/Graphene Hybrid Aerogel with High Compressibility, Conductivity, and "Sticky" Superhydrophobicity. *ACS Appl. Mater. Interfaces* **2014**, *6*, 3242–3249.
31. Zhang, L. L.; Zhao, X.; Stoller, M. D.; Zhu, Y.; Ji, H.; Murali, S.; Wu, Y.; Perales, S.; Clevenger, B.; Ruoff, R. S. Highly Conductive and Porous Activated Reduced Graphene Oxide Films for High-Power Supercapacitors. *Nano Lett.* **2012**, *12*, 1806–1812.
32. Zhou, H.; Zhu, S.; Hibino, M.; Honma, I.; Ichihara, M. Lithium Storage in Ordered Mesoporous Carbon (CMK-3) with High Reversible Specific Energy Capacity and Good Cycling Performance. *Adv. Mater.* **2003**, *15*, 2107–2111.
33. Frackowiak, E.; Gautier, S.; Gaucher, H.; Bonnamy, S.; Beguin, F. Electrochemical Storage of Lithium in Multiwalled Carbon Nanotubes. *Carbon* **1999**, *37*, 61–69.
34. Aurbach, D.; Ein-Eli, Y. The Study of Li-Graphite Intercalation Processes in Several Electrolyte Systems Using *In Situ* X-Ray Diffraction. *J. Electrochem. Soc.* **1995**, *142*, 1746–1752.
35. Fong, R.; von Sacken, U.; Dahn, J. Studies of Lithium Intercalation into Carbons Using Nonaqueous Electrochemical Cells. *J. Electrochem. Soc.* **1990**, *137*, 2009–2013.
36. Wang, H.; Yoshio, M. Carbon-Coated Natural Graphite Prepared by Thermal Vapor Decomposition Process, a Candidate Anode Material for Lithium-Ion Battery. *J. Power Sources* **2001**, *93*, 123–129.
37. Ohzuku, T.; Iwakoshi, Y.; Sawai, K. Formation of Lithium-Graphite Intercalation Compounds in Nonaqueous Electrolytes and Their Application As a Negative Electrode for a Lithium Ion (Shuttlecock) Cell. *J. Electrochem. Soc.* **1993**, *140*, 2490–2498.
38. Takami, N.; Satoh, A.; Hara, M.; Ohsaki, T. Rechargeable Lithium-Ion Cells Using Graphitized Mesophase-Pitch-Based Carbon Fiber Anodes. *J. Electrochem. Soc.* **1995**, *142*, 2564–2571.
39. Matsumura, Y.; Wang, S.; Mondori, J. Mechanism Leading to Irreversible Capacity Loss in Li Ion Rechargeable Batteries. *J. Electrochem. Soc.* **1995**, *142*, 2914–2918.
40. Yazami, R.; Deschamps, M. High Reversible Capacity Carbon-Lithium Negative Electrode in Polymer Electrolyte. *J. Power Sources* **1995**, *54*, 411–415.
41. Huang, X.; Yu, H.; Chen, J.; Lu, Z.; Yazami, R.; Hng, H. H. Ultrahigh Rate Capabilities of Lithium-Ion Batteries from 3D Ordered Hierarchically Porous Electrodes with Entrapped Active Nanoparticles Configuration. *Adv. Mater.* **2014**, *26*, 1296–1303.
42. Wu, H.; Chan, G.; Choi, J. W.; Yao, Y.; McDowell, M. T.; Lee, S. W.; Jackson, A.; Yang, Y.; Hu, L.; Cui, Y. Stable Cycling of Double-Walled Silicon Nanotube Battery Anodes Through Solid-Electrolyte Interphase Control. *Nat. Nanotechnol.* **2012**, *7*, 310–315.
43. Liu, N.; Lu, Z.; Zhao, J.; McDowell, M. T.; Lee, H.-W.; Zhao, W.; Cui, Y. A Pomegranate-Inspired Nanoscale Design for Large-Volume-Change Lithium Battery Anodes. *Nat. Nanotechnol.* **2014**, *9*, 187–192.
44. Chang, J.; Huang, X.; Zhou, G.; Cui, S.; Hallac, P. B.; Jiang, J.; Hurley, P. T.; Chen, J. Multilayered Si Nanoparticle/Reduced Graphene Oxide Hybrid As a High-Performance Lithium-Ion Battery Anode. *Adv. Mater.* **2014**, *26*, 758–764.
45. Ji, J.; Ji, H.; Zhang, L. L.; Zhao, X.; Bai, X.; Fan, X.; Zhang, F.; Ruoff, R. S. Graphene-Encapsulated Si on Ultrathin-Graphite Foam As Anode for High Capacity Lithium-Ion Batteries. *Adv. Mater.* **2013**, *25*, 4673–4677.